SPRINGER PROCEEDINGS IN PHYSICS 107

SPRINGER PROCEEDINGS IN PHYSICS

87 **Proceedings of the 25th International Conference on the Physics of Semiconductors**
Editors: N. Miura and T. Ando

88 **Starburst Galaxies**
Near and Far
Editors: L. Tacconi and D. Lutz

89 **Computer Simulation Studies in Condensed-Matter Physics XIV**
Editors: D.P. Landau, S.P. Lewis, and H.-B. Schüttler

90 **Computer Simulation Studies in Condensed-Matter Physics XV**
Editors: D.P. Landau, S.P. Lewis, and H.-B. Schüttler

91 **The Dense Interstellar Medium in Galaxies**
Editors: S. Pfalzner, C. Kramer, C. Straubmeier, and A. Heithausen

92 **Beyond the Standard Model 2003**
Editor: H.V. Klapdor-Kleingrothaus

93 **ISSMGE**
Experimental Studies
Editor: T. Schanz

94 **ISSMGE**
Numerical and Theoretical Approaches
Editor: T. Schanz

95 **Computer Simulation Studies in Condensed-Matter Physics XVI**
Editors: D.P. Landau, S.P. Lewis, and H.-B. Schüttler

96 **Electromagnetics in a Complex World**
Editors: I.M. Pinto, V. Galdi, and L.B. Felsen

97 **Fields, Networks, Computational Methods and Systems in Modern Electrodynamics**
A Tribute to Leopold B. Felsen
Editors: P. Russer and M. Mongiardo

98 **Particle Physics and the Universe**
Proceedings of the 9th Adriatic Meeting, Sept. 2003, Dubrovnik
Editors: J. Trampetić and J. Wess

99 **Cosmic Explosions**
On the 10th Anniversary of SN1993J (IAU Colloquium 192)
Editors: J. M. Marcaide and K. W. Weiler

100 **Lasers in the Conservation of Artworks**
LACONA V Proceedings, Osnabrück, Germany, Sept. 15–18, 2003
Editors: K. Dickmann, C. Fotakis, and J.F. Asmus

101 **Progress in Turbulence**
Editors: J. Peinke, A. Kittel, S. Barth, and M. Oberlack

102 **Adaptive Optics for Industry and Medicine**
Proceedings of the 4th International Workshop
Editor: U. Wittrock

103 **Computer Simulation Studies in Condensed-Matter Physics XVII**
Editors: D.P. Landau, S.P. Lewis, and H.-B. Schüttler

104 **Complex Computing-Networks**
Brain-like and Wave-oriented Electrodynamic Algorithms
Editors: I.C. Göknar and L. Sevgi

105 **Computer Simulation Studies in Condensed-Matter Physics XVIII**
Editors: D.P. Landau, S.P. Lewis, and H.-B. Schüttler

106 **Modern Trends in Geomechanics**
Editors: W. Wu and H.S. Yu

107 **Microscopy of Semiconducting Materials**
Proceedings of the 14th Conference, April 11–14, 2005, Oxford, UK
Editors: A.G. Cullis and J.L. Hutchison

Volumes 60–86 are listed at the end of the book.

A.G. Cullis J.L. Hutchison
(Eds.)

Microscopy of Semiconducting Materials

Proceedings of the 14th Conference, April 11–14, 2005, Oxford, UK

With 489 Figures

Springer

Professor A.G. Cullis
Department of Electronic
and Electrical Engineering
University of Sheffield
Mappin Street
Sheffield, S1 3JD, UK

Dr J.L. Hutchison
Department of Materials
University of Oxford
Parks Road
Oxford, OX1 3PH, UK

Published in association with Canopus Publishing Limited, Bristol, UK

ISSN 0930-8989

ISBN-10 3-540-31914-X Springer Berlin Heidelberg New York

ISBN-13 978-3-540-31914-6 Springer Berlin Heidelberg New York

Library of Congress Control Number: 2005939046

Springer is a part of Springer Science+Business Media.
springer.com

Printed in the UK

Cover concept: eStudio Calamar Steinen
Cover production: *design & production* GmbH, Heidelberg
Printing: Short Run Express, Exeter, UK

Printed on acid-free paper SPIN: 11610021 54/3141/mh 5 4 3 2 1 0

Preface

This volume contains the invited and contributed papers presented at the fourteenth conference on ‘Microscopy of Semiconducting Materials’ held at the University of Oxford on 11–14 April 2005. The event was organised with sponsorship by the Royal Microscopical Society, the Electron Microscopy and Analysis Group of the Institute of Physics and the Materials Research Society. This conference series focuses upon the most recent international advances in semiconductor studies carried out by all forms of microscopy: its truly international flavour was evident in that it was attended by delegates from approaching 20 countries.

Semiconducting materials allow the fabrication of advanced (opto)electronic devices ranging from ultrahigh speed FET and bipolar transistors to light emitters and detectors covering a very wide range of photon frequencies. However, to achieve the ultimate performance it is essential to optimise the structures of transistors with feature sizes often of less than 0.1 microns and also to understand the nature of, for example, advanced alloys of III-V and especially III-nitride materials. Efficient control of semiconductor processing on the nanometre scale is a vital concern and in order to achieve all of these goals, it is essential to exploit the techniques of advanced microscopy to characterise the materials at close to the atomic scale. For the highest spatial resolution, electron microscopy in its various forms provides the most wide-ranging information. Recent advances in instrumentation, from lens aberration correction in both TEM and STEM instruments and atomic level electron energy loss spectroscopy, to various scanned probe microscopy techniques, were all covered with both overviews and new results being presented. The work described at the present conference thus demonstrates the high level of on-going world-wide activity in all these areas.

Each camera-ready manuscript submitted for publication in this volume has been reviewed by at least two referees and modified accordingly; the editors are very grateful to the following colleagues for their rapid and careful refereeing work of the papers:

P E Batson, H Bender, P D Brown, N Browning, C B Carter, H Cerva, D Cherns, B Daudin, D Donnet, R Dunin-Borlowski, K Durose, M W Fay, K Furuya, F Glas, P J Goodhew, A Gustafsson, C Hetherington, C J Humphreys, P Koenraad, A Lauwers, S Mahajan, C Norenberg, Y Ohno, F M Ross, M Schowalter, E Spiecker, P Sutter, R Timm, T Walther, Y-L Wu.

The planning and organisation of an individual conference takes place over a two year cycle and work on the present meeting has been underpinned by Lucy Haworth, who deserves our very special thanks. We are also grateful for the assistance ably provided by Keith Fraser (University of Oxford) in meticulously correcting the proof copies of many manuscripts.

A G Cullis

October 2005 *J L Hutchison*

Contents

Part III Epitaxy: Growth and Defect Phenomena

Part IV High Resolution Microscopy and Nanoanalysis

Part V Self-Organised and Quantum Domain Structures

Part VI Processed Silicon and Other Device Materials

Part VIII Scanning Electron and Scanning Probe Advances

Part I

Epitaxy: Wide Band-Gap Nitrides

Structural properties of GaN quantum dots

B Daudin, J-L Rouvière, D Jalabert, J Coraux, V Favre-Nicolin, H Renevier, M H Cho[1], K B Chung[1], D W Moon[1], M G Proietti[2], J M Llorens[3], N Garro[3], A Cros[3] and A García-Cristóbal[3]

CEA/Grenoble, Department of Fundamental Research on Condensed Matter/ SP2M, 17 rue des Martyrs, 38054-Grenoble cedex 9, France
[1] Korea Research Institute of Standards and Science, Nano-Surface Group, 1 Doryong-Dong, Yuseong-Gu, Daejeon, 305-600, Korea (ROK)
[2] University of Zaragosa, Zaragosa, Spain
[3] Materials Science Institute, University of Valencia, P O Box 22085, E46071 Valencia, Spain

ABSTRACT: The strain state and the deformation profile of GaN quantum dots embedded in AlN have been measured by high resolution electron microscopy, medium energy ion scattering and grazing incidence X-ray diffraction. The results are compared with theoretical calculations, allowing one to conclude that GaN quantum dots experience a non biaxial strain which drastically decreases when going from the basal plane up to the apex of the dots. We also demonstrate that AlN is distorted in the surroundings of the dots, which provides the driving force for vertical correlation of GaN dots when the AlN spacer between successive planes is thin enough.

1. INTRODUCTION

The sustained interest for many years in quantum dots (QDs) of semiconductors relies on their three-dimensional carrier confinement properties which make them potentially very attractive for applications such as low threshold lasers as proposed by Arakawa and Sakaki (1982), single photon emission (Michler et al 2000, Santori et al 2000, Moreau et al 2001), quantum cryptography, single electron transistor (Fulton and Dolan 1987) or quantum computing. However, the practical realisation of devices simultaneously requires a good control of the size distribution of quantum dots and of their nucleation sites as well as of their structural, electrical and optical properties. Among the various parameters of interest, the strain state of QDs embedded in a matrix is an important one, which is closely related to their optical properties. This is of particular importance in the case of the III-nitride semiconductor family. As a matter of fact, due to the lack of a center of symmetry, the most usual wurtzite crystallographic phase of these materials exhibits both piezoelectric and spontaneous polarization. Because of the elevated value of the piezoelectric constants (see the calculations of Fiorentini et al (1999)), a huge internal electric field is currently observed in nitride heterostructures. It may be as high as several MV/cm in the case of GaN/AlN quantum wells, as shown by Adelmann et al (2003), or for GaN QDs embedded in AlN as studied by Simon et al (2003), Andreev and O'Reilly (2000 and 2001). Then, a strong red shift of the luminescence is induced as a consequence of the resulting quantum confined Stark effect, leading to luminescent emission at energies smaller than the GaN gap value for GaN/AlN quantum wells thicker than about 4 nm and for GaN/AlN QDs higher than 2.5 nm.

It is the objective of this article to report on the different experimental techniques allowing one to measure the strain in GaN quantum dots and to relate it with the optical properties. More precisely, high resolution transmission electron microscopy (HRTEM), X-ray diffraction under grazing incidence and medium energy ion scattering (MEIS) have been used. The satisfactory agreement between the experiments and theoretical calculations performed in the framework of the elastic continuum model has allowed us to conclude that GaN quantum dots embedded in AlN experience a combination of hydrostatic and biaxial strain leading to a gradient of elastic relaxation along the growth axis.

2. SAMPLES

The samples have been grown by plasma-assisted molecular beam epitaxy (PAMBE) in a commercial chamber equipped with standard effusion cells for Ga and Al. The N flux was produced by dissociation of N_2 in a radio-frequency plasma cell. The substrate was a 2-μm thick AlN layer deposited on sapphire as detailed by Shibata et al (2002). After a standard degreasing procedure and acid etching, the substrate was fixed with In on a molybdenum sample holder and introduced into the growth chamber. Prior to the growth of GaN QDs, an AlN buffer layer, about 100 nm thick, was grown in order to improve the surface quality. Then, GaN QDs were grown by depositing the equivalent of 6 monolayers (MLs) of GaN. The growth of the GaN QDs was performed according to the modified Stranski-Krastanow (SK) growth mode studied by Adelmann et al (2002) and Gogneau et al (2003): GaN was grown on AlN in Ga-rich conditions which results in the formation of a Ga bilayer on the surface as described by Northrup et al (2000). This metal layer stabilizes the 2D GaN layer and inhibits the 2D/3D transition, characteristic of the usual SK growth mode, which was observed by Daudin et al (1997) when growing GaN in N-rich conditions. After depositing GaN, both Ga and N fluxes were suppressed. Then, the thermal evaporation of the stabilizing Ga bilayer was followed by a reorganization of the 2D GaN layer and the formation of 3D islands as described in detail by Gogneau et al (2003). The samples used in the present study were a superlattice of vertically correlated GaN QDs (for HRTEM) and single planes of GaN dots uncapped or capped with an increasing quantity of AlN (for MEIS and X Rays diffraction). Details on the samples are given in the relevant sections.

3. RESULTS

3.1 High Resolution Electron Microscopy

Once deposited, GaN quantum dots can be covered by AlN in order to recover a smooth surface. Next, the operation can be repeated, allowing one to grow superlattices of planes of GaN QDs in an AlN matrix. Depending on the thickness of the AlN spacer, GaN QDs can be correlated or not, according to the model proposed by Tersoff et al (1996). In this work, it was established that the deformation of the surrounding matrix by dots actually leads to a modulation of the elastic potential and to the preferential nucleation of the upper dots just above the lower ones.

Figure 1 (which is part of a 2Kx2K image taken with a CCD camera) zooms on a GaN QD which is part of a superlattice of planes of GaN QDs embedded in AlN, with an AlN spacer thin enough (about 10 nm) to result in vertical correlation of dots.

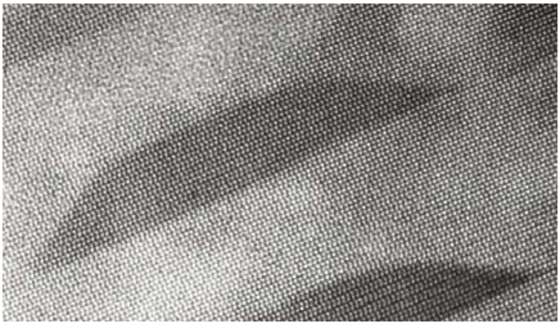

Fig. 1: HRTEM image of GaN quantum dots embedded in AlN taken along a <2,-1,-1,0> direction

A quantitative analysis of the whole image has been performed using the geometrical phase analysis technique (Hytch et al 1998, Rouvière and Sarigiannidou, unpublished). The result is displayed in Fig.2a and 2b which are maps of the local *c* and *a* lattice parameters, respectively. It demonstrates that compressed GaN QDs induce strain in the surrounding AlN matrix. In particular, it is found that AlN above the dots exhibits an expanded *a* lattice parameter, that is to say that AlN is in tension and constitutes a privileged nucleation centre for the upper GaN dots, which leads to the building-up of vertical correlation of GaN QDs.

Combining the results in Fig.2a and 2b, it is possible to extract a map of *c/a* ratio value which is shown in Fig. 2c. An average value of 1.64 is found in the GaN QDs, allowing one to conclude that GaN QDs are relaxed to a large extent, as *c/a* would be 1.69 in the hypothesis of a biaxial strain and equal to 1.625 in a bulk GaN crystal (see Fig. 6).

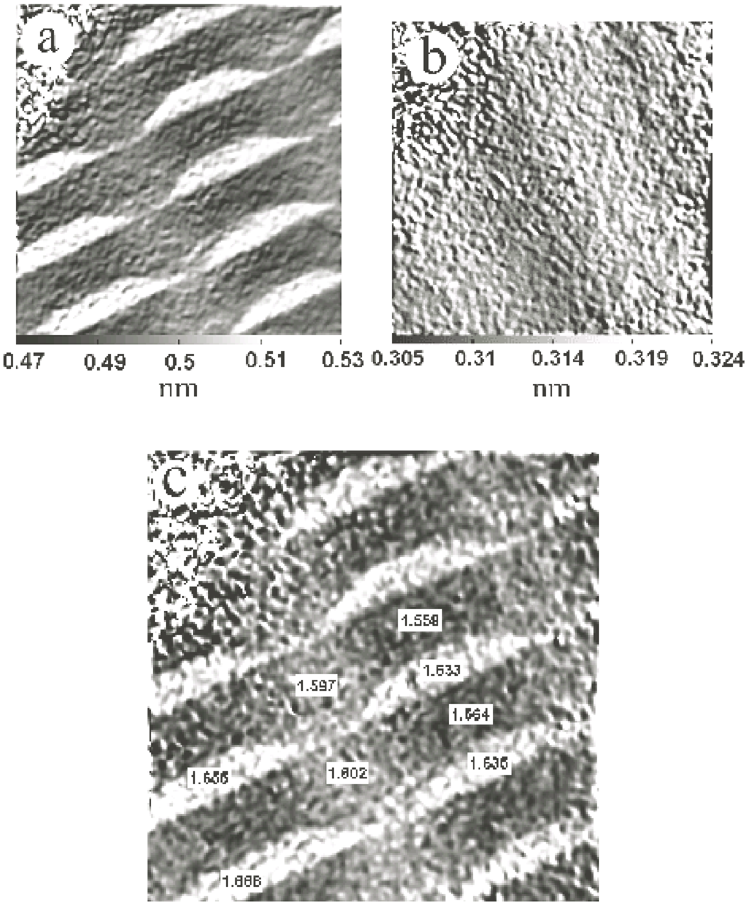

Fig. 2: Maps of the whole 2Kx2K CCD image shown in Fig. 1. (a) map of the *c* lattice parameter; (b) map of the *a* lattice parameter; (c) *c/a* mapping extracted from results displayed in Fig. 2a and 2b. Note that the relaxed values of *c* and *a* are 0.5185 nm and 0.3189 nm, respectively, leading to a *c/a* ratio of 1.625

3.2 Medium Energy Ion Scattering (MEIS)

A more detailed knowledge of deformation profile in GaN QDs can be obtained by medium energy ion scattering (MEIS) experiments which were performed using a 101 keV incident H^+ ion beam, $\theta_{in} \sim 7°$ off the [0001] direction (see Fig. 3). The energy and angular distribution of scattered protons were measured with a two-dimensional detector described by Tromp et al (1991), whose energy resolution, $\Delta E/E$, is about 3×10^{-3} and angular resolution is 0.1°. The scattering geometry was chosen in order to observe a range of ± 10° around the [1-101] direction in the (11-20) plane.

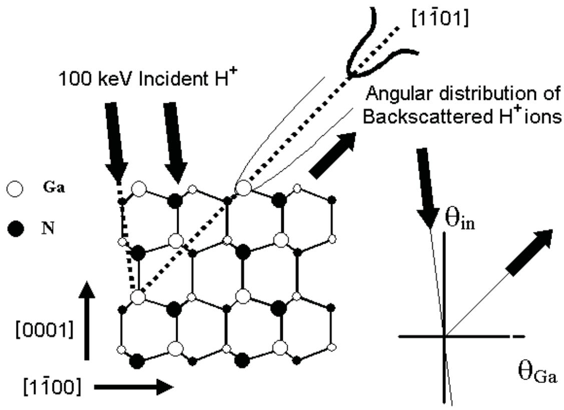

Fig. 3: Scheme of the scattering geometry in the (11-20) plane for medium ion energy scattering experiments.

Then, by measuring the backscattered proton energy as a function of scattering angle, it is possible to determine the change in shadowing direction as a function of depth which is related, in the case of GaN QDs, to their deformation profile along the growth axis. Figure 4 shows the result in the case of uncovered QDs. A similar experiment has been performed in the case of one plane of GaN QDs covered with 20 monolayers of AlN. The deformation profile extracted from the data is shown in Fig. 5. It is worth noting that, at the top of dots, the *c/a* ratio is equal to the value corresponding to relaxed GaN. However, it must be recalled at this stage that MEIS does not allow one to independently determine *c* and *a*, preventing the conclusion that GaN QDs are completely relaxed at their tops.

In order to better understand the MEIS results, simulations of the strain distribution in a single lattice-mismatched wurtzite GaN/AlN quantum dot have been performed. The calculations have been done in the framework of the elastic continuum theory by using the inclusion method developed by Eshelby (1957), which considers the dot as a misfitting inclusion (GaN) in an infinite matrix (AlN). In order to describe the dot geometry, we have adopted a truncated cone shape with height 3 nm, and base and top diameters equal to 13.3 and 3 nm, respectively, leading to an aspect ratio of 0.22. Furthermore, the dot is assumed to lie on a 0.5-nm-thick two-dimensional wetting layer. The output of the calculations is the full inhomogeneous strain tensor $\varepsilon_{ij}(\mathbf{r})$, from which the local strained values of *a* and *c* are obtained as $a(\mathbf{r}) = (1+\varepsilon_{pp}(\mathbf{r}))a_0$ and $c(\mathbf{r}) = (1+ \varepsilon_{zz}(\mathbf{r}))c_0$, respectively. This procedure does not take into account the distortion caused by the shear strains, which are found to be very small throughout most of the dot volume.

The detailed results of the calculation are reported elsewhere by Jalabert et al (2005). In order to facilitate the comparison with MEIS data, the theoretical depth profile of *c/a* extending from z = -0.5 nm (wetting layer underneath the QD) to z = 3 nm (top of the QD) is shown in Fig. 6. The values represented have been obtained by averaging the calculated *c/a* over the dot cross section perpendicular to the *z* axis.

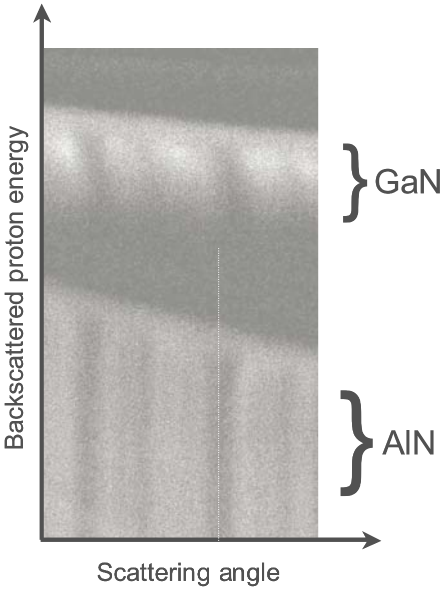

Fig. 4: Backscattering proton energy as a function of scattering angle for one plane of uncovered GaN QDs on AlN. The dotted line is an eye guide to visualise the channelling dip in AlN substrate. Note the deviation from this line in the GaN region, which puts in evidence the gradient of deformation in GaN QDs as a function of depth

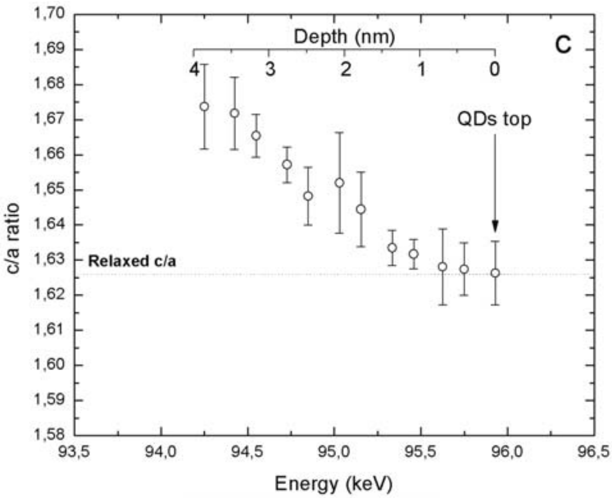

Fig. 5: *c/a* ratio as a function of depth in GaN QDs covered with 20 MLs of AlN (about 5 nm)

From the satisfactory agreement between calculations and experimental results shown in Fig. 5, we conclude that the general trends of the measured gradient of *c/a* through the QD are well reproduced in the theoretical analysis. As a matter of fact, the calculations establish that, inside the dot, the in-plane lattice parameter *a* is always compressed, although to a different values depending on the position, whereas the parameter *c* is expanded in the base and compressed at the top of the dot as commented in details by Jalabert et al (2005). This behaviour is very sensitive to the dot morphology and aspect ratio and results in a strain state quite inhomogeneous. As a whole, this strain state drastically differs from the biaxial strain characteristic of two-dimensional films, which is frequently invoked to describe the deformation of self-assembled QDs. It is worth noting that in the region of the AlN/GaN interface, the calculated *c/a* value of 1.675 agrees very well with the experimental value and still lies relatively away from the biaxial value.

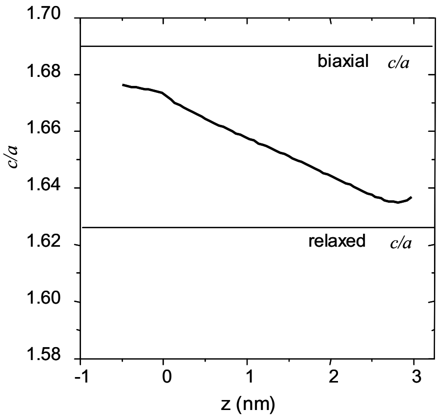

Fig. 6: calculated depth profile of the in-plane averaged *c/a*. The two full lines indicates the value of *c/a* corresponding to relaxed, unstrained GaN and to two-dimensional GaN layer biaxially strained to AlN, respectively.

3.3 Grazing Incidence X-ray Scattering

An alternative approach to determine the strain state of QDs consists of performing anomalous diffraction at grazing incidence (GIDAFS). As schematised in Fig. 7, taking advantage of the reduced penetration depth for α_i smaller than the critical angle value allows one to measure one single plane of capped/uncapped dots. Furthermore, the X-ray energy can be tuned across the absorption Ga K-edge where the Ga atoms scattering power is strongly modified and diffraction becomes chemically selective, giving direct information on composition. This technique has been applied to the case of a single plane of uncapped/capped GaN QDs which were studied as a function of the thickness of capping layer, namely 0 (S1967), 2 (S1956), 5 (S158), 10 (S1959) and 20 (S1961) MLs, to elucidate also the role of the AlN capping layer on the QDs strain field.

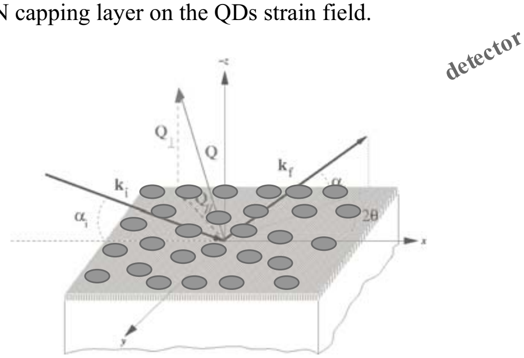

Fig. 7: Schematics of a grazing incidence diffraction experiment. α_i is of the order of the critical angle so that penetration of XRays is reduced to some tens of nm allowing one to measure only one plane of capped/uncapped dot

The experiment was performed at the Ga K-edge (10.367 keV) at the French Collaborative Research Group beamline BM2 at ESRF, by using a 8-circles diffractometer equipment. We measured the diffuse scattering intensity, close to the in-plane (30-30) Bragg reflection of the AlN substrate as a function of energy and close to the Ga K-edge. The incidence angle was α_i=0.15º, lower than the critical angle α_c=0.20º, for which the total reflection regime takes place. We recorded two different kinds of scan a) h-scans in the range of 2.9-3 with k=l=0 for 12 different energy values varying from 10.268 to 10.418 keV, i.e. close to the Ga K-edge (see Fig.8) b) energy scans at fixed Q-vector, corresponding to the QDs maximum contribution to the diffuse scattering (i.e. at the maximum of the partial structure factor of the Ga atoms profile, F_A, recovered from the multiwavelength h-scans, as discussed by Letoublon et al (2004). The energy scans (shown in Fig. 9) were recorded in quite a large energy interval, about 1000eV, to allow quantitative analysis of both the edge and extended oscillations region.

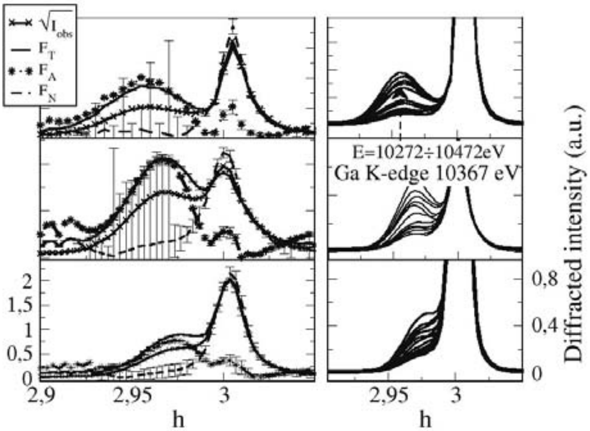

Fig. 8: hkl-scans for samples s1967 (no AlN capping: upper), s1956 (2ML AlN capping: middle), s1959(10ML AlN capping: lower). Right panels: diffracted intensity for different energies of the incident photons. Left panels: Multiwavelength anomalous diffraction (MAD) extraction of the partial structure factors F_A and F_T

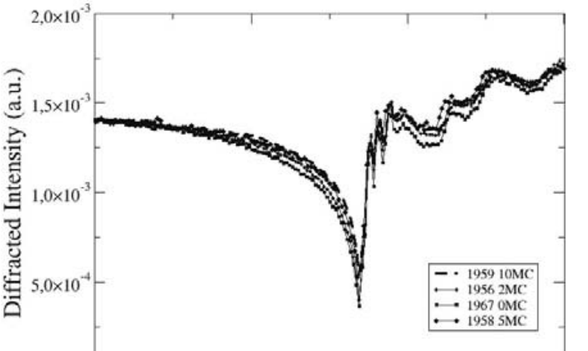

Fig. 9: GIDAFS spectra for 0, 2, 5 and 10 ML AlN capping, measured at top of F_A.

From the hkl scans we can recover, without any starting model, the structure factor F_A , i.e. the contribution of the Ga atoms to diffraction, and determine the in-plane lattice parameter *a* from the F_A

maximum position. One can see in Fig. 8 that the F_A maximum shifts towards higher h values corresponding to lower *a* values as the capping layer thickness increases, that is, we monitor the effect of the capping layer on the in-plane QDs' strain. The lattice parameter *a* is reported in table 1 where we see that it drops from 3.157 Å to 3.147Å. These values stay in between of the GaN and AlN bulk *a* values, 3.189 Å and 3.112 Å, respectively, i.e., the QDs exhibit an average partial in-plane relaxation.

Analysis of the EDAFS oscillations provides the microscopic local environment of the Ga resonant atom: interatomic distances, *c* lattice parameter, in the QDs.

The results are shown in Table 1 and in Fig.10 where the background subtracted EDAFS oscillations are compared with best fit curve for sample s1967 (uncovered QDS).

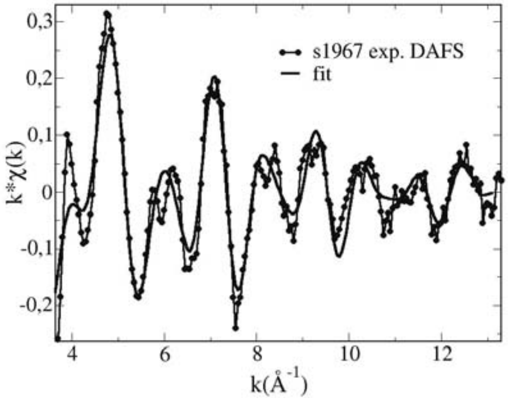

Fig. 10: Experimental EDAFS for the free standing QDs sample (s1967), compared with the best fit result.

We find a tendency to an over-strained regime (with respect to the purely biaxial strain case) that suggests a complex mechanism of strain accommodation and deserves further investigations.

	Bulk	***GaN/AlN***	***S1967 (1pl. no cap)***	***S1956 (1pl. + 2MLcap)***	***S1958 (1pl. + 5MLcap)***	***S1959 (1pl. + 10MLcap)***
R_1(Ga-N) (Å)	-	-	1.93	1.94	1.94	1.94
σ_1^2 (Å)^2	-	-	2x10^{-3}	4x10^{-3}	4x10^{-3}	1x10^{-3}
R_2 (Ga-Ga) // (Å)	3.188	3.11	3.156(diff.)	3.147 (diff.)	3.149(diff)	3.14 (diff.)
σ_2^2 (Å)^2	-	-	6x10^{-3}	8x10^{-3}	4x10^{-3}	7x10^{-3}
R_2(Ga-Ga)⊥ (Å)	3.18	-	3.190	3.18	3.180	3.186
c	5.186	5.26	5.25±0.02	5.23±0;03	5.22±0.02	5.25±0.04
c/a	1.626	1.69	1.66	1.66	1.66	1.67

Table 1 : EDAFS best fit values for interatomic distances and Debye-Waller factors obtained by IFEFFIT minimisation (Newille et al. 1995) using theoretical fitting standards provided by FEFF8 code developed by Ankudinov et al (1998). The amplitude and phase correction factors have been obtained by cristallographic analysis of the DAFS lineshape (Proietti et al 1999). R_1 and R_2 refer to interatomic distances, (diff.) refers to diffraction results

From results in Table 1, it appears that the *c/a* ratio as determined by EDAFS is about 1.66, clearly between the 1.626 value of relaxed bulk GaN and the 1.69 value of GaN biaxially strained on

AlN. As viewed by MEIS, 1.66 corresponds to the *c/a* value in the lower part of uncapped and AlN-capped GaN QDs (see Jalabert et al (2005) and Fig. 5). By comparison, EDAFS experiments provide an average value of *c/a*. Actually, due to the facetted shape of GaN QDs (see Daudin et al 1997), most of the diffracting volume corresponds to the base of the truncated hexagonal pyramid, giving more weight to the contribution of this part of the dots, consistent with experimental results. By contrast, HRTEM experiments potentially provide a detailed mapping of *c/a* parallel and perpendicular to the growth axis. However, the analysis may be intrinsically perturbed by thin foil effects resulting from sample preparation. As a whole, it appears that the combined use of the three techniques described here is complementary and eventually leads to a realistic knowledge of the deformation of GaN QDs embedded in AlN.

4. CONCLUSION

In conclusion, it has been shown that the complementary use of HREM, MEIS and GIDAFS allows one to measure the strain state and the deformation profile of semiconductor quantum dots with a spatial resolution in the monolayer range. It has been found that GaN QDs experience a non biaxial strain and significantly distort the surrounding AlN matrix, which provides the driving force for dot vertical correlation. The experimental results are in reasonable agreement with those of calculations performed in the framework of elastic continuum theory. We conclude that the dots are partly relaxed, and that capping them with AlN leads to a progressive increase of their relaxation/deformation stage.

ACKNOWLEDGEMENTS

We acknowledge Y Genuist, Y Curé and M Lafossas for their technical help.

REFERENCES

Adelmann C, Gogneau N, Sarigiannidou E, Rouvière J L and Daudin B 2002 Appl. Phys. Lett. **81**, 3064

Adelmann C, Sarigiannidou E, Jalabert D, Hori Y, Rouvière J L and Daudin B 2003 Appl. Phys. Lett. **82**, 4154

Andreev A D and O'Reilly E P 2000 Phys. Rev. B **62** 15851

Andreev A D and O' Reilly E P 2001, Appl. Phys. Lett. **79**, 521

Ankudinov A L, Ravel B and Rehr J J 1998 Phys. Rev. B **58** 7565

Arakawa Y and Sakaki H 1982 Appl. Phys. Lett. **40**, 939

Daudin B, Widmann F, Feuillet G, Samson Y, Arlery M and Rouvière J L 1997 Phys. Rev. B **56**, 7069

Eshelby J D 1957 Proc. R. Soc. London, Ser. A **241**, 376

Fiorentini V, Bernardini F, Della Sala F, Di Carlo A and Lugli P 1999, Phys. Rev. B **60** 8849

Fulton T A and Dolan G J 1987 Phys. Rev. Lett. **59**, 109

Gogneau N, Jalabert D, Monroy E, Shibata T, Tanaka M and Daudin B 2003 J. Appl. Phys **94**, 2254

Hÿtch M J, Snoeck E and Kilaas R 1998 Ultramicroscopy **74** 131

Jalabert D, Coraux J, Renevier H, Daudin B, Mann-Ho C, Kwun-Bum C, Moon D W, Llorens J M, Garro N, Cros A and García-Cristóbal A 2005 Physical Review B, in press

Letoublon A, Favre-Nicolin V, Renevier H, Proietti M G, Monat C, Gendry M, Marty O and Priester C 2004 Phys. Rev. Lett. **92** 186101

Michler P, Kiraz A, Becher C, Schoenfeld W V, Petroff P M, Lidong Zhang, Hu E, and Imamoglu A 2000 Science **290**, 2282

Moreau E, Robert I, Manin L, Thierry-Mieg V, Gérard J M, and Abram I 2001 Phys. Rev. Lett. **87**, 183601

Newville M, Ravel b, Haskel D, Rehr J J and Stern E A 1995 Physica B **208-209**, 154

Northrup J E, Neugebauer J, Feenstra R M and Smith A R 2000 Phys. Rev. B **61**, 9932

Rouvière J L and Sarigiannidou 2005, unpublished

Santori C, Pelton M, Solomon G, Dale Y, and Yamamoto Y 2000 Phys. Rev. Lett. **86**, 1502

Simon J, Pelekanos N T, Adelmann C, Martinez-Guerrero E, Andre R, Daudin B, Le Si Dang, and Mariette H 2003 Phys. Rev. B **68** 35312

Proietti M G, Renevier H, Hodeau J L, Garcia J, Bérar J F and Wolfers P 1999 Phys. Rev. B **59**, 5479
Shibata T, Asai K, Nagai T, Sumiya S, Tanaka M, Oda O, Miyake H and K. Hiramatsu K 2002 Mat. Res. Soc. Symp. Proc. 693, 541
Tersoff J, Teichert C and Lagally M G 1996 Phys. Rev. Lett. **76**, 1675 Tromp R M, Copel M, Reute M C, von Hoegen M H , Speidell J and Koudis R 1991 Rev. Sci. Instrum. **62**, 2679
Wang Y P and Meltzer R S 1992 Phys. Rev. B **45**, 10119

Stranski-Krastanov growth for InGaN/GaN: wetting layer thickness changes

N K van der Laak, R A Oliver, M J Kappers, C McAleese and C J Humphreys

Department of Materials Science and Metallurgy, University of Cambridge, Pembroke Street, Cambridge CB2 3QZ, United Kingdom

ABSTRACT: We have investigated InGaN nanostructures grown by atmospheric pressure metal-organic vapour phase epitaxy. The variation of the 3D nanostructure density and the wetting layer thickness with growth time have been studied. The nanostructure density was found to saturate with increasing growth time, but unexpectedly, the nanostructure size was also seen to stabilise. We have used high-resolution transmission electron microscopy (HRTEM) to further investigate the wetting layer growth and quantify changes with InGaN growth time.

1. INTRODUCTION

The self-assembled growth of nanostructures following the Stranski-Krastanov (SK) growth mode has been achieved for a number of material systems including Si_xGe_{1-x}/Si (Eaglesham and Cerullo 1990), $In_xGa_{1-x}As/GaAs$ (Ruvimov et al 1995), and GaN/AlN (Chamard et al 2004). Growth of InGaN nanostructures has also been achieved by both molecular beam epitaxy (MBE) and metal-organic vapour phase epitaxy (MOVPE). Typical SK growth in InGaAs/GaAs materials systems follows a regime in which the nanostructure density increases with growth time. At a certain wetting layer thickness misfit dislocations are introduced and the nanostructures coalesce resulting in a transition back to 2D growth (Tachibana et al 1999). The latter authors have reported growth of InGaN/GaN quantum dots at atmospheric pressure by MOVPE. 3D islands were reported to form on top of a 2D wetting layer (WL) akin to SK growth, and the density of the 3D islands was seen to increase with growth time. However, unlike the InGaAs/GaAs system, coherent nanostructures were observed with continued growth time. Here we report our observations of atmospheric MOVPE growth of InGaN/GaN nanostructures.

2. EXPERIMENTAL

Two sample sets were grown for this work in a 6 x 2” CCS-Thomas Swan MOVPE reactor. The first series comprised uncapped InGaN epilayers of increasing thickness and were characterised using a Veeco Dimension 3100 atomic force microscope (AFM) in tapping mode. The second series comprised similar InGaN layers which were capped immediately after growth with 7.5 nm of GaN deposited at the InGaN growth temperature and were used for cross-sectional HRTEM analysis. The HRTEM analysis was performed using a JEOL 4000-EX II HRTEM. A fuller description of the growth can be in found in Oliver et al (2005).

3. RESULTS

Figure 1 shows a series of AFM images of InGaN epilayers with different growth times. After 15 s of InGaN growth (Fig. 1a), flat terraces with decorated step edges and a low nanostructure density of about 8.9 x 10^7 cm^{-2} is observed. After 31 s of growth time (Fig. 1b) the nanostructure density increases quickly to approximately 2 x 10^9 cm^{-2} and then appears to stabilise with longer

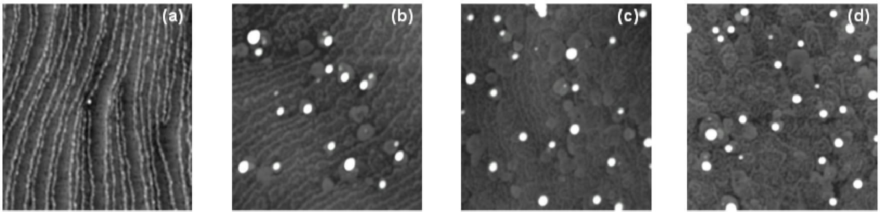

Fig. 1: 1 µm × 1 µm AFM scans of InGaN epilayers grown on GaN (a) Growth time, t = 15 s, image height, h = 1.56 nm, (b) t = 31 s, h = 15.97 nm, (c) t = 62 s, h = 22.35 nm (d) t = 93 s, h = 13.89 nm. In all the images, some nanostructures are seen as bright white features as the displayed contrast has been adjusted in order to allow the detailed structure of the wetting layer to be easily seen.

growth times (Fig. 2). The modal nanostructure height is also observed to increase sharply, then plateau (Fig. 3) which suggests that the 3D island growth stabilises after 31 s of InGaN growth time.

This in itself is surprising as the amount of InGaN material in the system is increasing, yet neither continued island growth nor coalescence of the nanostructures as seen in the InGaAs/GaAs system occurs. A closer examination of the AFM images shows that at 31 s of InGaN growth time 2D islands are now present. The density of these islands increases up to 125 s of InGaN growth where the wetting layer is dominated by irregular 2D islands, completely covering the terrace structure seen in Fig. 1a.

This change in the wetting layer was further investigated by HRTEM. A series of capped InGaN layers for 31, 46, 62, and 93 s were studied in cross-section to deduce if any changes in the WL could be seen and quantified. Lattice fringe images were obtained by tilting the sample 7 ° off the [11-20] zone axis, so that the systematic (0002) row of reflections was excited. The crystal was oriented at the symmetry position and the objective aperture selected the three beams, 0, (0002) and (000-2) to form the lattice image. Under certain conditions such as on-zone axis, lattice fringes can be observed in the high-resolution images. The nominal thickness can be determined by measuring across successive (0002) interplanar distances along the growth direction of the material. The (0002) interplanar spacing, *d*, for GaN was taken to be 2.593 Å and this was used to determine the distance over 10 lattice fringe spacings in the underlying GaN layer, so that an internal reference scale was established for each sample. The distance across the InGaN WL was measured and the absolute distance was determined using the GaN internal reference scale. Once an absolute scale for each sample is determined, the number of pixels spanning the area of interest, i.e. the InGaN epilayer, can be correlated to the scale and the thickness determined. This procedure was performed consistently for each sample and the average WL thickness (and hence the total amount of material in the WL) was determined. Figs. 4a-d show typical HRTEM images for the different InGaN growth times. As the WL has some roughness, the mean thickness was determined using measurements from several

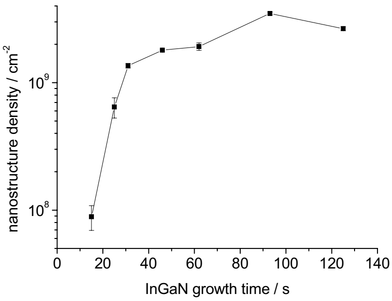

Fig. 2: Variation of InGaN nanostructure density with growth time.

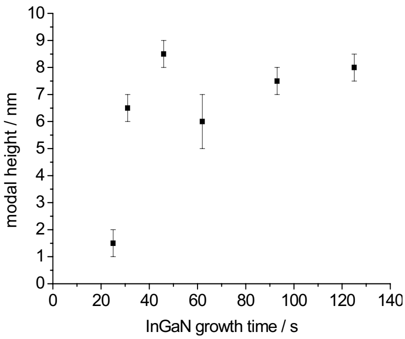

Fig. 3: Variation of the modal InGaN nanostructure height with growth time.

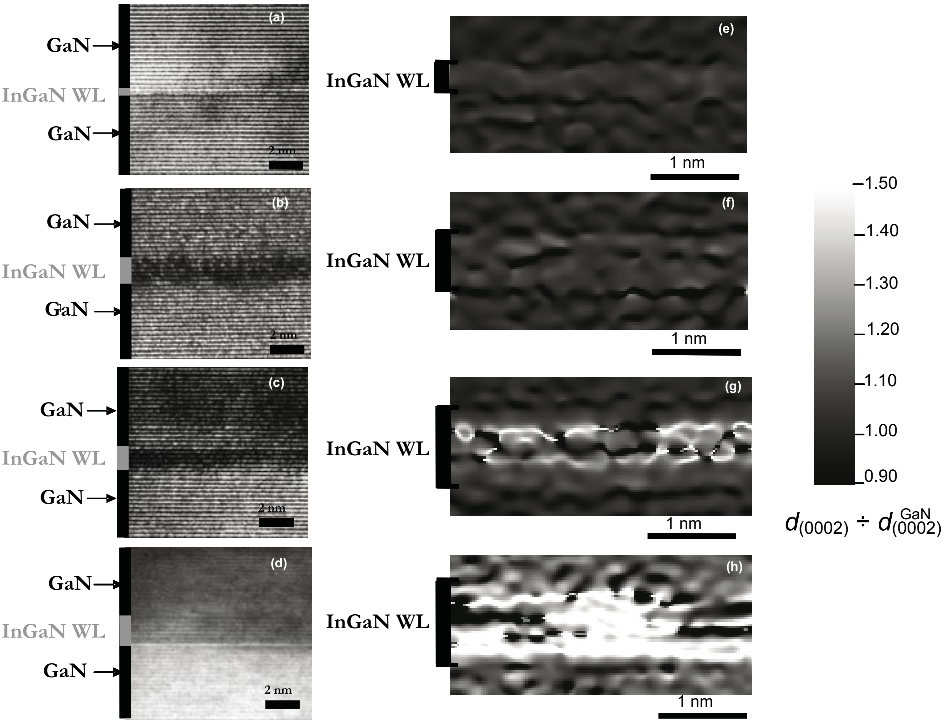

Fig. 4: (a-d) HRTEM lattice fringe images showing a typical wetting layer region for 31, 46, 62, and 93 s of InGaN growth time, respectively and, (e-h) lattice parameter maps extracted from the images demonstrating changes in the wetting layer thickness for 31, 46, 62, and 93 s of InGaN growth time, respectively.

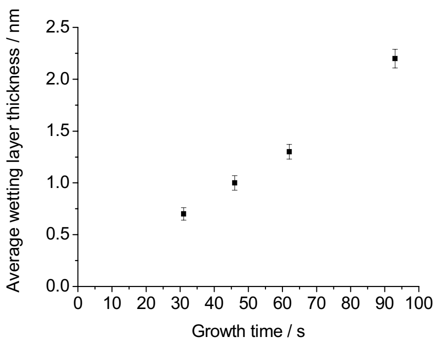

Fig. 5: Variation of the InGaN wetting layer thickness as measured by HRTEM on capped InGaN layers.

images and this mean, which can be seen to increase with growth time across the range of samples, is shown in Fig. 5.

Lattice parameter maps were also used to characterise the WL thicknesses. Figs. 4e-h show the lattice parameter maps extracted from the same regions displayed in the HRTEM images. The maps show the ratio of the measured $d_{(0002)}$ lattice spacing as a function of the GaN $d_{(0002)}$ lattice spacing. As the d spacing for InGaN is larger than that for GaN, the InGaN WL will appear as brighter regions in the lattice parameter maps. The maps indicate that, as the growth time increases, the InGaN WL thickness increases. What is also apparent, is that as the InGaN growth time is increased the intensity of the bright regions increases. This may be attributed to the increasing strain contribution within the InGaN WL and suggests that more indium is being incorporated with increasing InGaN growth time. This is not surprising as our SIMS analysis of InGaN quantum wells shows that the amount of indium incorporated in the well increases with well thickness.

4. DISCUSSION

The data shows that after approximately 31 s the nanostructure density saturates and plateaus, while the modal height remains stable. This indicates that the nanostructure distribution stabilises. The TEM investigation has shown that the WL increases in thickness as the InGaN growth time is increased. This is consistent with the AFM observations which show an increase of 2D islands under the same growth conditions. However, if the WL were to increase and no material were added to the nanostructures, the 2D layer would eventually cover the nanostructures and both the size and density would decrease. Hence, it is suggested that material may be added simultaneously to the WL layer and the 3D nanostructures in order to maintain the density and height distribution.

This deviation from the normal SK paradigm could be explained by the relatively low temperatures and high pressures at which the growth was carried out. The WL appears to grow by partial formation and merging of flat 2D islands. At low temperatures and high pressures the adatom mobility is reduced, hence the adatoms diffusing across the WL surface may form clusters that grow by accretion. As the 3D island density is relatively low (ca. 2×10^9 cm^{-2}) distances between the islands are relatively large, so the 3D nanostructures may grow in a similar fashion to the WL by adatoms impinging close to or on the islands. This would suggest that the growth mode is kinetically controlled. However, recent results have suggested that the crystal structure of the 3D islands is zincblende, not wurtzite, which may alter our understanding of the growth process.

5. CONCLUSIONS

In summary, we have shown that, in atmospheric pressure MOVPE growth of InGaN on GaN, the wetting layer thickness increases via the formation and merging of 2D islands while the 3D nanostructure density and height increase sharply and then stabilise for longer InGaN growth times. It has been suggested that slow kinetically controlled growth may account for these observations; however we have noted that a phase change from wurtzite to zincblende may also play a role.

REFERENCES

Chamard V, Schülli T, Metzger T H, Sarigiannidou E, Rovuière J-L, Tolan M, Adelmann C

Eaglesham D J and Cerullo M 1990 Phys. Rev. Lett. **64**, 1943

Oliver R A, Kappers M J, Humphreys C J Humphreys and Briggs G A D 2005 J. Appl. Phys. 97, 013707

Ruvimov S, Werner P, Scheerschmidt K, Gösele U, Heydenreich J, Richter U, Ledentsov N N, Grundmann M, Bimberg D, Ustinov V M, Egorov A Yu, Kop'ev P S and Alferov Zh I 1995 Phys. Rev. B. **51**, (20), 14776

Tachibana K, Someya T and Arakawa Y 1999 Appl. Phys. Lett. **74**, 383